


RESEARCH

Open Access



# Microstructural integrity of the locus coeruleus and its tracts reflect noradrenergic degeneration in Alzheimer's disease and Parkinson's disease

Chen-Pei Lin<sup>1,2\*</sup> , Irene Frigerio<sup>1,2</sup>, John G. J. M. Bol<sup>1</sup>, Maud M. A. Bouwman<sup>1,2</sup>, Alex J. Wesseling<sup>1,2</sup>, Martin J. Dahl<sup>3,4</sup>, Annemieke J. M. Rozemuller<sup>5,6</sup>, Ysbrand D. van der Werf<sup>1,2,7</sup>, Petra J. W. Pouwels<sup>2,8</sup>, Wilma D. J. van de Berg<sup>1,6</sup> and Laura E. Jonkman<sup>1,2,6</sup>

## Abstract

**Background** Degeneration of the locus coeruleus (LC) noradrenergic system contributes to clinical symptoms in Alzheimer's disease (AD) and Parkinson's disease (PD). Diffusion magnetic resonance imaging (MRI) has the potential to evaluate the integrity of the LC noradrenergic system. The aim of the current study was to determine whether the diffusion MRI-measured integrity of the LC and its tracts are sensitive to noradrenergic degeneration in AD and PD.

**Methods** Post-mortem in situ T1-weighted and multi-shell diffusion MRI was performed for 9 AD, 14 PD, and 8 control brain donors. Fractional anisotropy (FA) and mean diffusivity were derived from the LC, and from tracts between the LC and the anterior cingulate cortex, the dorsolateral prefrontal cortex (DLPFC), the primary motor cortex (M1) or the hippocampus. Brain tissue sections of the LC and cortical regions were obtained and immunostained for dopamine-beta hydroxylase (DBH) to quantify noradrenergic cell density and fiber load. Group comparisons and correlations between outcome measures were performed using linear regression and partial correlations.

**Results** The AD and PD cases showed loss of LC noradrenergic cells and fibers. In the cortex, the AD cases showed increased DBH + immunoreactivity in the DLPFC compared to PD cases and controls, while PD cases showed reduced DBH + immunoreactivity in the M1 compared to controls. Higher FA within the LC was found for AD, which was correlated with loss of noradrenergic cells and fibers in the LC. Increased FA of the LC-DLPFC tract was correlated with LC noradrenergic fiber loss in the combined AD and control group, whereas the increased FA of the LC-M1 tract was correlated with LC noradrenergic neuronal loss in the combined PD and control group. The tract alterations were not correlated with cortical DBH + immunoreactivity.

**Conclusions** In AD and PD, the diffusion MRI-detected alterations within the LC and its tracts to the DLPFC and the M1 were associated with local noradrenergic neuronal loss within the LC, rather than noradrenergic changes in the cortex.

\*Correspondence:

Chen-Pei Lin

c.p.lin@amsterdamumc.nl

Full list of author information is available at the end of the article



© The Author(s) 2024. **Open Access** This article is licensed under a Creative Commons Attribution 4.0 International License, which permits use, sharing, adaptation, distribution and reproduction in any medium or format, as long as you give appropriate credit to the original author(s) and the source, provide a link to the Creative Commons licence, and indicate if changes were made. The images or other third party material in this article are included in the article's Creative Commons licence, unless indicated otherwise in a credit line to the material. If material is not included in the article's Creative Commons licence and your intended use is not permitted by statutory regulation or exceeds the permitted use, you will need to obtain permission directly from the copyright holder. To view a copy of this licence, visit <http://creativecommons.org/licenses/by/4.0/>. The Creative Commons Public Domain Dedication waiver (<http://creativecommons.org/publicdomain/zero/1.0/>) applies to the data made available in this article, unless otherwise stated in a credit line to the data.

**Keywords** Locus coeruleus, Noradrenergic degeneration, Alzheimer's disease, Parkinson's disease, Diffusion MRI, Post-mortem, Histopathology

## Background

The noradrenergic system, ascending from the locus coeruleus (LC) and projecting to limbic and cortical brain regions [1], supports cognitive processes including attention, memory and executive functions via the release of noradrenaline [2–4]. Dysregulation of the LC-noradrenergic system leads to deterioration of the aforementioned cognitive functions [5] and manifests in the pathophysiology of both Alzheimer's disease (AD) and Parkinson's disease (PD) [2, 4]. Restoring the LC-noradrenergic system has thus become an important target in both diseases [6–8], and neuroimaging biomarkers assaying the LC-noradrenergic system for monitoring disease progression and potential treatment effects are needed [9, 10].

Magnetic resonance imaging (MRI) tools assessing the integrity of the LC are continuously in development [10, 11]. For instance, LC-sensitive imaging showed reduced LC signal intensity in both AD and PD patients compared to controls [12–16]. Although the biophysiological interpretation of the LC signals requires further investigation [17, 18], assessments of LC integrity have shown potentials for patient stratification and predicting a noradrenergic treatment response in relation to behavioral improvements [19, 20]. Another MRI technique, diffusion MRI, is able to assess the microstructural integrity of the white and grey matter with its derivatives, fractional anisotropy (FA) and mean diffusivity (MD) [21–26]. Increased LC FA and decreased MD in the aging population compared to young controls, as well as their association with a decline in memory performance, highlight the capability of diffusion MRI to capture LC microstructural integrity [26]. Furthermore, a recent double-blind randomized three-way crossover study showed great potential of diffusion MRI markers for patient stratification: they identified likely responders from non-responders to noradrenergic treatments in PD with an accuracy of 77%–79% [27]. In a randomized, double-blind placebo-controlled crossover study, PD patients administered with atomoxetine showed increased FA in white matter tracts, which was associated with improved response inhibition [28], suggesting that diffusion measures assessing the integrity of white matter tracts may be a potential predictor of behavioral recovery. Altogether, these findings suggest that developing and validating diffusion MRI markers targeting the LC-noradrenergic system are beneficial for assessing noradrenergic treatment effects in AD and PD.

Profound LC-noradrenergic neuronal and fiber loss, as well as neuropathological burdens of hyperphosphorylated-tau (p-tau), amyloid-beta (A $\beta$ ) and alpha-synuclein ( $\alpha$ -syn), have been described in AD and PD, accompanied by reduced cortical noradrenergic innervation and in turn reduced cortical noradrenaline levels [29, 30]. The vulnerability of noradrenergic axons stems from their nature—they are long and highly branched with less myelination that allows noradrenergic innervation and efficient neurotransmission in the neocortex. In AD, this diminished cortical noradrenaline, especially in the hippocampus, has been associated with memory deficits [31]. In PD and PD dementia (PDD), a reduction in noradrenergic fibers has been shown in the primary motor cortex (M1) compared to controls [32], suggesting an involvement of noradrenergic denervation in motor deficits [33]. In addition, cognitive impairment has been linked to reduced noradrenaline levels in the prefrontal cortex (PFC) and anterior cingulate cortex (ACC) in both PD and PDD [7, 34]. These postmortem studies suggest that degeneration of tracts from the noradrenergic LC to the hippocampus, PFC, ACC and M1 may contribute to cognitive and/or motor symptoms in AD and PD(D). Despite the noradrenergic system being implicated in AD and PD, currently, only a limited number of studies have investigated the *in vivo* integrity of the LC-to-cortex tracts in AD and controls [25, 35, 36], and no research has been done in PD. Moreover, no studies have validated their results with the ground truth of human LC-noradrenergic neuronal and fiber loss.

We previously developed a pipeline for post-mortem *in situ* MRI in combination with immunohistochemistry to study the correlation between MRI measures and neuronal markers in the same brain donor(s) [37]. Here, we used this pipeline to study whether diffusion MRI measures of microstructural alterations within the LC and the cortical projections from LC reflect the severity of LC-noradrenergic degeneration in AD and PD. We hypothesized that: (i) AD and PD cases show altered diffusion MRI measures in the LC and its projections to the PFC, ACC, M1 and hippocampus, (ii) these MRI-measured alteration(s) correlate with LC-noradrenergic neuronal loss and/or reduced noradrenergic innervation in the cortex. This study may aid the development of noradrenergic-sensitive *in vivo* MRI markers for assessing the degeneration of the LC-noradrenergic system.

**Methods**

**Donor inclusion**

A total of 31 clinically defined and pathologically confirmed brain donors were included in the current post-mortem MRI and pathology study: 9 amnesic AD, 14 PD, as well as 8 age- and sex-matched control donors. During life, all donors provided written informed consent for the use of their brain tissue and medical records for research purposes. AD and PD donors were included in collaboration with the Netherlands Brain Bank (NBB; [http://brain](http://brainbank.nl)

[bank.nl](http://brainbank.nl)). PD and PDD were diagnosed based on clinical presentations according to the Movement Disorder Society clinical diagnostic criteria [38–40]. Disease durations were extracted from the clinical files of the donors. The control donors were included at the Department of Anatomy and Neurosciences, Amsterdam UMC, following the Normal Aging Brain Collection Amsterdam (NABCA; <http://nabca.eu>) pipeline [37]. All donors underwent post-mortem in situ MRI with subsequent brain autopsy and dissection of brainstem, limbic and cortical regions

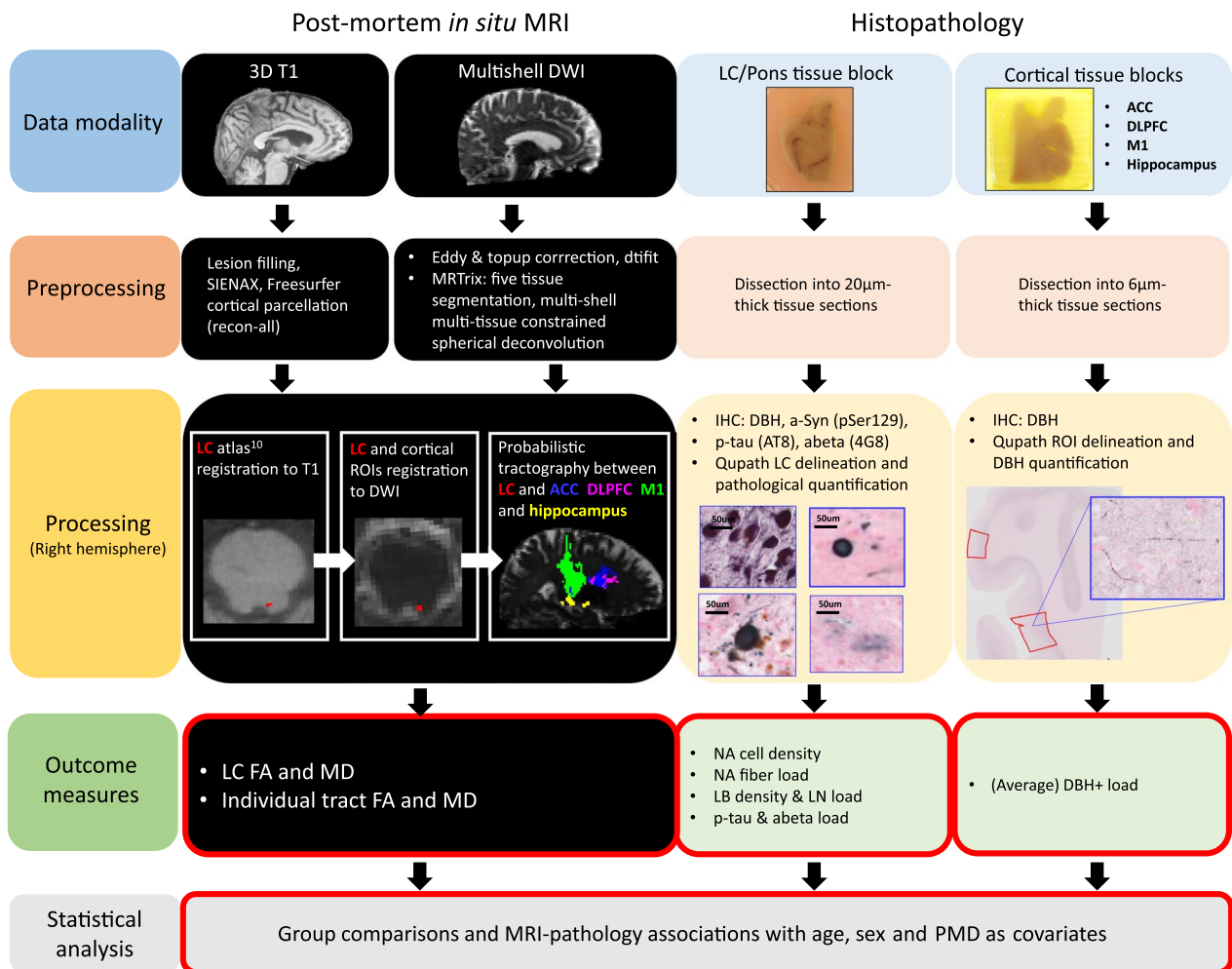


**Fig. 1** Flow chart of the study. After donor inclusion, post-mortem in situ 3D T1 and multi-shell diffusion MRI images were collected and (pre) processed: the LC was segmented [44] and the LC tracts to the anterior cingulate cortex (ACC, blue tract), the dorsolateral prefrontal cortex (DLPFC, purple tract), the primary motor cortex (M1, green tract) and the hippocampus (yellow tract) were reconstructed, deriving the FA and the MD of the LC and its tracts. Autopsy and brain dissection were performed after the in situ MRI scans. Brain tissue blocks were formalin-fixed for 4 weeks, then dissected and paraffin-embedded. Next, 20-µm-thick sections were processed for immunohistochemistry for dopamine-beta hydroxylase (DBH), phosphorylated Ser129  $\alpha$ -synuclein (pSer129- $\alpha$ syn), phosphorylated-tau (p-tau) and amyloid- $\beta$  ( $\beta$ ), and imaged using a whole-slide scanner. Immunoreactivity in regions of interest were analyzed using Qupath, deriving the LC-noradrenergic cell density and fiber load, Lewy body (LB) density and Lewy neurite (LN) load. The group comparisons between AD, PD and controls were investigated with general linear models and the association between MRI and pathology markers was investigated with linear regression models, including age, sex and post-mortem delay as covariates. Abbreviations: DWI, diffusion-weighted tensor imaging; LC, locus coeruleus; NA, noradrenergic; IHC, immunohistochemistry; FA, fractional anisotropy; MD, mean diffusivity; LB, Lewy body; LN, Lewy neurite; PMD, post-mortem delay

based on the Brain Net Europe (BNE) and NABCA protocol [37, 41]. Neuropathological diagnosis was performed by an expert neuropathologist (AJMR) according to the international guidelines of BNE. The study design is summarized in Fig. 1.

### MRI acquisition

Post-mortem MRI data were acquired through in situ (brain still in cranium) scanning on a whole-body 3T MR scanner (Signa-MR750, General Electric Medical Systems, Chicago, IL) with an eight-channel phased-array head-coil [37]. T1-weighted images (T1w) were acquired using a sagittal 3D T1-weighted fast spoiled gradient echo sequence (FSPGR) with the following parameters: repetition time (TR)/echo time (TE)/inversion time (TI)=7/3/450 ms, flip angle=15°, slice thickness=1 mm, in-plane resolution=1.0×1.0 mm<sup>2</sup>. A sagittal 3D fluid attenuation inversion recovery (FLAIR) sequence was acquired with TR/TE/TI=8000/130/2000–2250 ms, slice thickness 1.2 mm, and in-plane resolution=1.11×1.11 mm<sup>2</sup>. In addition, the inversion time of the FLAIR sequence was optimized per case to account for variable CSF suppression due to post-mortem delay (PMD; time between death and MRI scanning). Diffusion-weighted images (DWI) were acquired with a multi-shell single-spin echo-planar imaging sequence (TR=7651 ms, TE=104 ms, 1.75×1.75 mm<sup>2</sup> in-plane resolution, slice thickness 2 mm) with 89 interleaved directions (30  $b=1000$  s/mm<sup>2</sup> and 59  $b=2000$ s/mm<sup>2</sup>) and 6 non-diffusion-weighted volumes ( $b=0$  s/mm<sup>2</sup>). To allow for geometric distortion correction, b0 volumes with reversed phase-encode direction were obtained.

### MRI analysis

#### *Structural image processing and LC atlas registration*

To minimize the impact of age-related white matter abnormalities (e.g., vascular change) on automated segmentations, the 3D T1 images were lesion-filled [42], as previously described. Subsequently, normalized brain volumes of the whole brain, white matter, and gray matter were estimated from 3D T1 images using SIENAX [43], FMRIB Software Library (FSL) tools version 6.0.4 (<https://fsl.fmrib.ox.ac.uk/fsl/>). To delineate the LC of each case, an existing binary LC atlas of the entire LC from Dahl et al. [11, 44] was used. First, for each case, the whole brain was skull-stripped and co-registered to standard space (MNI-ICBM 152 linear, 0.5 mm) using a template-based procedure implemented in Advanced Normalization Tools (ANTs, version 2.1) [45, 46]. The inverse of the transformation matrices was then applied to the LC meta mask to warp it to native space with nearest neighbor interpolation, deriving the entire LC in subject T1 space. The complete script can

be found in the Additional file 1. In addition, to derive the cortical regions of interest (ROIs), namely the ACC, dorsolateral prefrontal cortex (DLPFC), M1 and hippocampus, each hemisphere was parcellated into 34 anatomical cortical regions using the Desikan–Killiany atlas with Freesurfer, version 7.0 (<http://surfer.nmr.mgh.harvard.edu>) [47]. The reconstructed datasets were visually inspected, and segmentation errors were corrected. The LC and cortical ROIs of individual brain scans were transformed from 3D T1 to diffusion space: the DWI images were first co-registered to 3D T1 to generate the transformation matrices, which were inverted and used for registering the ROIs to diffusion space for further probabilistic tractography [48]. LC registration from the atlas to diffusion space is illustrated in Additional file 1: Fig. S1. All cases were visually inspected for the location of the LC in both 3D T1 and DWI, from the dorsal end of the inferior colliculus to the floor of fourth ventricle, to ensure its correct anatomical location.

#### *DWI pre-processing, microstructural assessment and probabilistic tractography*

DWI was first denoised using the dwidenoise tool in MRtrix3, to improve the generally low signal-to-noise ratio in DWI [49]. Subsequently, the susceptibility-induced off-resonance field was estimated and corrected from pairs of images with opposite phase-encoding directions using topup, and eddy current-induced distortion correction was applied with the FSL software suite [50]. To assess the microstructural integrity of the LC and its tracts, we fitted the tensor to  $b=2000$  s/mm<sup>2</sup> data to determine FA and MD using FSL DTIFIT [51]. FA and MD of  $b=1000$  s/mm<sup>2</sup> data were also fitted for validation. The FA and MD maps of both shells were registered to 3D T1 with trilinear interpolation, and average values of the LC were extracted in subject T1 space.

To assess the LC tract microstructural integrity, we reconstructed the LC tracts in the right hemisphere, as the tissue blocks and subsequent pathological outcome measures were only available from this hemisphere. Tractography was performed with MRtrix3, using anatomically-constrained probabilistic tractography (ACT). To achieve this, 3D T1 images were segmented based on five-tissue response functions, and transformed to DWI space, providing information on streamline propagation and termination during tractography. In addition, the fiber orientation in each voxel was estimated with Multi-Shell Multi-Tissue Constrained Spherical Deconvolution (MSMT-CSD) [52, 53]. Embedded within the tractography function (tckgen), ACT was performed with the LC



as the seed ROI and the cortical ROIs (ACC, DLPFC, M1, and hippocampus) as separate target ROIs, resulting in four tracts: LC-ACC, LC-DLPFC, LC-M1 and LC-hippocampus, with 5000 streamlines per tract with a maximum length of 250 mm. In addition, to ensure that streamlines are within the right hemisphere, a left hemisphere mask was generated, and used as an exclusion mask during ACT. Thereafter, the FA and MD of individual tracts were determined based on the probability-weighted mean along the tract.

## Histology and immunohistochemistry processing

### Tissue sampling

After post-mortem *in situ* MRI, donors were transported to the mortuary for craniotomy. The left hemisphere was instantly dissected and snap-frozen in liquid nitrogen, and stored for molecular and biochemical analysis. The right hemisphere was fixed in 4% formalin for four weeks. Subsequently, the right hemisphere was dissected based on the BNE sampling protocol to extract the LC, ACC, DLPFC, M1 and hippocampus (including the entorhinal cortex, parahippocampal and fusiform gyrus, as described previously [54, 55]). The rostral LC neurons project to the forebrain regions, hippocampus and septum; whereas the middle and caudal portions of the LC project to the cerebellum, basal ganglia and spinal cord [56, 57]. Therefore, the rostral LC was included in the current study in order to examine the noradrenergic projections to the ACC, DLPFC, M1 and hippocampus. All tissue blocks were paraffin-embedded and stained with (immuno)histochemistry [37, 41].

### Immunohistochemistry

For detailed methods, see Additional file 1. In brief, paraffin-embedded tissue blocks of the LC were cut into  $4 \times 20 \mu\text{m}$ -thick consecutive sections, and stained with monoclonal rabbit anti-dopamine-beta hydroxylase (DBH, dilution 1:400, Abcam, Cambridge, UK), rabbit anti-phosphorylated-Ser129  $\alpha$ -syn (clone EP1536Y, dilution 1:4000, Abcam), mouse anti-p-tau (clone AT8, dilution 1:800, ThermoFisher, Pittsburgh, PA) or mouse anti-A $\beta$  (clone 4G8, dilution 1:5000, BioLegend, San Diego, CA) antibody. The paraffin-embedded cortical tissue blocks, the ACC, DLPFC, M1 and hippocampus, were cut at  $6 \mu\text{m}$  and processed for immunohistochemistry with rabbit anti-DBH (dilution 1:400, Abcam). The DLPFC sections were stained with an alternative DBH antibody for validation (dilution 1:100, Novus, Cambridge, UK, Additional file 1). The primary antibodies were incubated at  $4^\circ\text{C}$  overnight and visualized with Vector SG grey (Vector, Newark, CA), 3,3'-diaminobenzidine (DAB, Sigma-Aldrich, Darmstadt, Germany), or DAB+Nickel, followed by counter-staining with nuclear

fast red (Vector). The sections were dehydrated in a series of ethanol, xylene, and then mounted with Entellan.

### ROI delineation and pathological quantification

Immunostained sections of the LC were digitally scanned with the Vectra Polaris Quantitative Pathology Imaging System (PerkinElmer, Waltham, MA) at  $200\times$  magnification with a  $20\times$  objective. Immunostained sections of the cortical regions were scanned with Olympus VS200 (Evident, Japan) using a focus map grid to capture the DBH-stained fibers. Qupath Software Version 0.2.3 [58] was used to process the scanned images, perform the delineation of the LC and cortical regions, and finally quantify the noradrenergic neurons and fibers, as well as  $\alpha$ -syn, p-tau and A $\beta$  pathological load [58]. Based on a previously described delineation method [56, 59, 60], the LC delineation was defined by placing a  $2.5 \text{ mm}^2$  sampling grid at the center of the cluster of neuromelanin-containing cells on DBH-stained sections. With the aid of neighboring anatomical landmarks, namely the fourth ventricle, mesencephalic trigeminal nucleus and its tract, and superior cerebellar peduncle [30], the sampling grid was placed at a similar level of the LC in each case, independent of the neuromelanin-containing cell load (Additional file 1: Fig. S2). The same sampling grid was transferred to consecutive stained sections of  $\alpha$ -syn, p-tau and A $\beta$ . Noradrenergic neurons, represented by DBH-positive (DBH<sup>+</sup>) neurons, and immunoreactivity of  $\alpha$ -syn, p-tau and A $\beta$ , were quantified using the in-house QuPath scripts. For cortical regions stained with DBH, ROIs containing all cortical layers were delineated in straight areas of the cortex, to avoid over- or under-estimation of immunoreactivity in sulci and gyri, respectively [61, 62]. Hippocampal sections were segmented according to the method described by Adler et al., in which CA1 to CA4 regions were included and combined [55]. In cortical regions, we quantified structures with highly intense DBH<sup>+</sup> signals that form elongated, as well as dot-like structures, representing the traveling and cross-sectional noradrenergic axons, respectively (Additional file 1: Fig. S3). These intense signals inevitably include few punctate staining of DBH, we thus took the outcome of DBH quantification as DBH<sup>+</sup> load (%).

Detailed description of the quantification can be found in Additional file 1: Methods and Figs. S2 and S3. To summarize, the immunohistochemistry outcome measures included were DBH-positive (DBH<sup>+</sup>) noradrenergic cell density (count/ $\text{mm}^2$ ), noradrenergic fiber load (% area), Lewy body (LB) density (count/ $\text{mm}^2$ ), Lewy neurite (LN) load (% area), p-tau load (% area) and A $\beta$  load (% area) within the LC, as well as the DBH<sup>+</sup> load (% area) within each cortical area.

**Statistical analysis**

Statistical analysis was performed using IBM SPSS 22.0 for Windows (SPSS, Inc., Chicago, IL). All statistical variables were tested for normality. Chi-square tests were used to analyze group difference between AD, PD and control donors for categorical variables. General linear models (GLM) were used for the aforementioned group differences in MRI-derived outcome measures (FA and MD of LC, as well as FA and MD of individual tracts), and histopathological outcome measures. We applied linear regression models to examine the associations between the above-mentioned MRI and histopathology-derived outcome measures. Age, sex and PMD were included as covariates in all analysis. The regression models were performed in two ways: (1) within the whole cohort; (2) only within the control + AD or control + PD groups. Group comparisons and correlation analysis were followed by false discovery rate (FDR) correction for multiple comparisons [63]. Graphical illustrations were made with Biorender (<https://biorender.com/>), R (<https://www.rstudio.com/>) and Graphpad (<https://www.graphpad.com/>). Since our PD group included PD and PDD, for the clarity purpose, we labeled PD in dark blue and PDD in light blue in figures.

**Results**

**Clinical, radiological and pathological characteristics**

Group demographics are summarized in Table 1. For detailed donor information, see Additional file 1: Table S1. For clinical characteristics, compared to controls, no differences in age, sex or PMD were found for AD and PD cases. Compared to AD, PD cases were older ( $P=0.028$ ) and had a longer disease duration ( $P=0.012$ ). For the radiological characteristics of normalized total grey matter volume, the AD group showed a lower volume compared to the PD and control groups ( $P=0.004$  and  $P=0.013$ , respectively), while no differences were found between PD and control cases. No difference was found for normalized total brain or white matter volume. For pathological characteristics, the AD cases showed higher Thal and Braak stages of neurofibrillary tangle compared to both PD and control cases (both  $P<0.001$ ), while no difference was found between PD and control cases. All PD cases had Braak LB stage 6, while both AD and control cases had Braak LB stage 0.

**Microstructural integrity of the LC and its tracts in AD and PD**

The average LC volumes in both T1 and DWI space (before normalization to the intracranial brain volume)

**Table 1** Demographics, clinical, radiological and pathological characteristics of included cohort

	Control	AD	PD
<i>Clinical characteristics</i>			
Number of cases	8	9	14 (8 PD and 6 PDD)
Sex, male/female (%male)	5/3 (63%)	7/2 (78%)	10/4 (71%)
Age at death, years	73 ± 11 (range 57–85)	64 ± 10 (53–84) <sup>#</sup>	75 ± 6 (62–90)
Disease duration, years	–	9 ± 6 <sup>#</sup>	15 ± 4
Post-mortem delay (h:min)	7:18 ± 2:14	8:12 ± 0:58	7:06 ± 1:52
<i>Radiological characteristics</i>			
Normalized brain volume (ml)	1468.7 ± 69.1	1391.8 ± 132.4	1417.9 ± 90.1
Normalized grey matter volume (ml)	732.4 ± 52.9	649.2 ± 64.6 <sup>*,#</sup>	700.6 ± 47.0
Normalized white matter volume (ml)	736.4 ± 37.8	742.7 ± 105.8	717.4 ± 73.5
<i>Pathological characteristics</i>			
Thal phase (n)	8	9 <sup>**,##</sup>	14
0/1/2/3/4/5	1/6/0/0/1/0	0/0/0/1/4/4	0/7/3/4/0/0
Braak neurofibrillary tangle stage (n)	8	9 <sup>**,##</sup>	14
0/1/II/III/IV/V/VI	2/2/1/3/0/0/0	0/0/0/0/1/5/3	0/1/10/3/0/0/0
Braak Lewy body stage (n)	8	9	14
0/1/2/3/4/5/6	8/0/0/0/0/0/0	9/0/0/0/0/0/0	0/0/0/0/0/0/14

Mean ± SD; h, hour; min, minutes

\* $P<0.05$  compared to controls

\*\* $P<0.001$  compared to controls

<sup>#</sup>  $P<0.05$  compared to PD

<sup>##</sup>  $P<0.001$  compared to PD

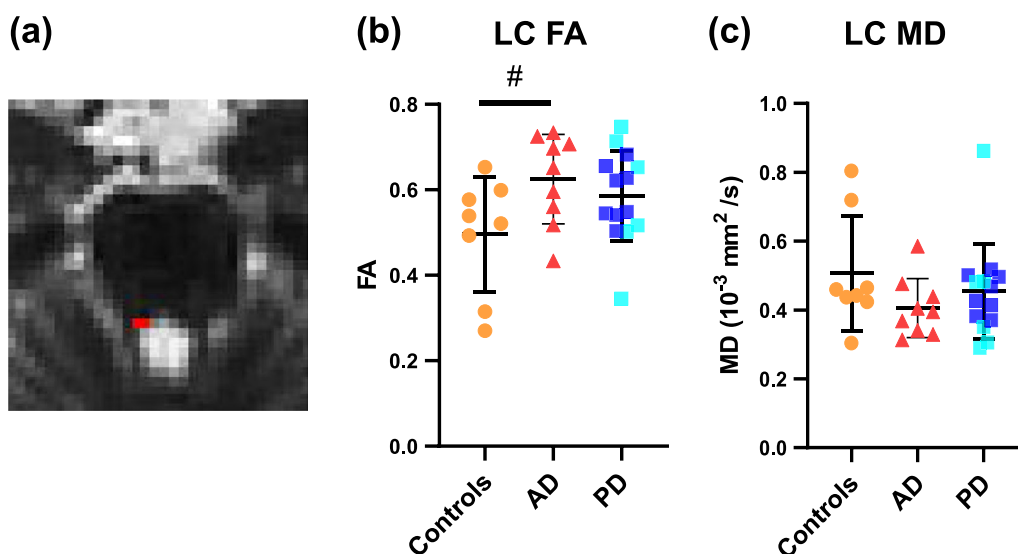


**Fig. 2** LC microstructural integrity in controls, AD and PD. **a** The LC (red) of the right hemisphere in DWI in a radiological view. **b** Increased LC FA ( $P=0.040$ , uncorrected) was found in AD cases compared to controls. **c** No significant difference in LC MD was found between groups. Within the PD group, PD cases are labeled with darker blue, whereas PDD cases are labeled with lighter blue. # $P < 0.05$ , uncorrected

in each group can be found in Additional file 1: Table S2. The resulting LC masks are LC-enriched, as the LC volumes were slightly larger than LC volume estimation in stereological studies [56, 64]. On T1 MRI, the LC volume did not differ between groups (AD:  $26.78 \pm 7.33 \text{ mm}^3$ , PD:  $25.12 \pm 8.85 \text{ mm}^3$ , controls:  $26.88 \pm 5.65 \text{ mm}^3$ ). On diffusion MRI, the AD group showed higher FA compared

to controls ( $P=0.040$ , uncorrected, Fig. 2a), though this significance did not survive correction for multiple comparisons. No difference in FA was found between PD and controls or between AD and PD. The MD showed no difference between groups (Fig. 2). FA and MD of the LC extracted from  $b=1000$  shell showed similar results; a higher FA of the LC (trend-level) was found in AD

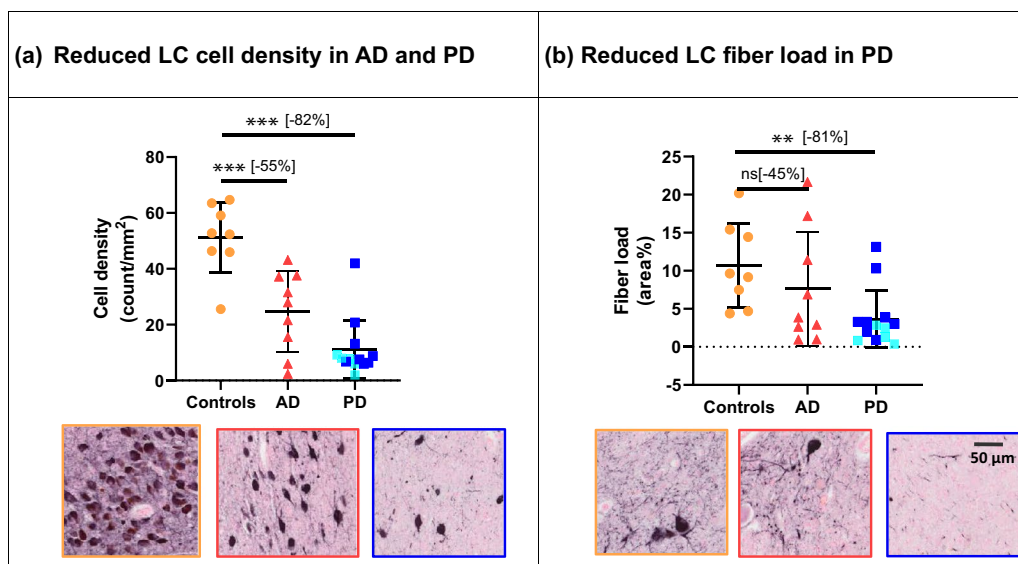


**Fig. 3** Noradrenergic cell density and fiber load within the LC of controls, AD and PD cases. **a** Noradrenergic cell density was lower in AD and PD compared to control cases. **b** Noradrenergic fiber load was lower in PD compared to control cases. Scale bar, 50 µm for all images. Within the PD group, PD cases are labeled with darker blue, whereas PDD cases are labeled with lighter blue. ns, not significant. \*\* $P < 0.01$  FDR-corrected, \*\*\* $P < 0.001$  FDR-corrected

compared to controls, while no differences were found between PD and controls. No group difference was found for MD (Additional file 1: Table S3). As for the tracts between the LC and cortical regions, no significant group differences were found in either FA or MD (Additional file 1: Table S4).

### Severity of LC neuronal loss and pathological burden in AD and PD

Both the AD and the PD cases showed noradrenergic neuronal loss within the LC (Fig. 3). Compared to controls, the AD cases showed a 55% decrease of noradrenergic cell density ( $P=0.0002$ , FDR-corrected) and a trend of noradrenergic fiber loss ( $-45%$ ,  $P=0.067$ , uncorrected). In turn, the PD cases showed a 82% decrease of noradrenergic cell density ( $P<0.0001$ , FDR-corrected) and a 81% decrease of noradrenergic fiber load ( $P=0.003$ , FDR-corrected), compared to controls. Compared to the AD cases, the PD cases showed a trend of reduced noradrenergic cell density ( $-61%$ ,  $P=0.051$ , uncorrected), but no significant difference in noradrenergic fiber load ( $P=0.124$ ) (Fig. 3). Both AD and control cases showed a large within-group variability in LC noradrenergic cell density and fiber loads, whereas PD cases showed less within-group variability (Fig. 3).

With regard to the pathological burden within the LC, both A $\beta$  and p-tau pathology were found in the AD cases, while only some p-tau pathology was found in PD and control cases (Additional file 1: Fig. S4).  $\alpha$ -Syn pathology in the forms of LB and LN was found in PD cases and not in controls. Only one AD case showed a LB in the LC (Additional file 1: Fig. S5), but did not meet the criteria of Braak LB stage 1. We found no correlations between noradrenergic loss within the LC and the pathological burden in AD or PD (Additional file 1: Table S5). We also examined the association with disease duration but found no correlations for noradrenergic cell density or fiber load (Additional file 1: Table S6). The AD group consisted of early- and late-onset (EOAD and LOAD) cases. The EOAD cases carrying homozygous *APOE4* had more severe neuronal loss (Additional file 1: Fig. S6).

### Reduced cortical noradrenergic innervation in PD, but increased innervation in AD

The noradrenergic innervation of the ACC, DLPFC, M1 and hippocampus was compared between groups (Additional file 1: Fig. S7). Noradrenergic fibers were identified based on an intense DBH<sup>+</sup> staining and varicosities (shape of bouton) along the axons, which were present in both deep and superficial layers of the cortex. Consistent with previous literature [65], we observed relatively weak DBH staining in dendritic, somatic and axonal synapses (punctate staining as shown in Additional file 1: Fig.

S3). In the ACC, M1 and hippocampus, more elongated noradrenergic fibers were observed in both superficial and deep cortical layers of controls compared to AD and PD donors. In addition, AD and PD donors showed more fibers with pathological features such as larger varicosities along the axons, and tangled or clustered fiber structures. In the DLPFC, surprisingly, we observed increased noradrenergic fibers and (synaptic) innervation in both deep and superficial cortical layers of the AD donors. The staining patterns resembled sprouting fibers and synaptic staining surrounding the soma of cortical neurons (Additional file 1: Fig. S8). This observation was confirmed with another commercial antibody polyclonal rabbit anti-DBH (dilution 1:100, Novus, Cambridge, UK; Additional file 1: Methods, Fig. S9).

On a statistical level, the PD cases showed a 45% decrease of DBH<sup>+</sup> load in the ACC compared to AD ( $P=0.061$ , uncorrected, Fig. 4a), and a 34% decrease of DBH<sup>+</sup> load in the M1 compared to controls ( $P=0.03$ , uncorrected, Fig. 4c). No group differences were found between AD and controls in these two regions (Fig. 4). For the hippocampus, no group differences were found between any pair of groups (Fig. 4d). In the DLPFC, as expected from the descriptive results of DBH-immunoreactivity, the AD cases showed higher DBH<sup>+</sup> load compared to controls and PD (increase by 78% and 87%, respectively,  $P=0.006$  and  $P=0.007$ , both FDR-corrected), while no difference was found between PD and controls (Fig. 4b). As a previous study indicated an age effect on the degeneration of the noradrenergic cells and fibers in the LC and cortical ROIs [66], we also examined the correlation between age and DBH-immunoreactivity in the LC and all cortical regions, and found no age effect in our cohort (Additional file 1: Table S7).

### Changes in cortical noradrenergic innervation are associated with LC neuronal loss in AD and PD

Since we found that the DLPFC and M1 showed altered noradrenergic innervation in AD and PD, respectively, we hypothesized that these alterations may stem from noradrenergic cell and/or fiber loss within the LC. We found that the increased DBH<sup>+</sup> load in the DLPFC was correlated with decreased LC noradrenergic cell density in the combined AD and control group ( $r=-0.52$ ,  $P=0.036$ , FDR-corrected), but not in the AD group alone. In the M1 region, trend-level correlations were found between reduced DBH<sup>+</sup> load in the M1 and reduced LC noradrenergic cell density in the combined PD and control group ( $r=0.47$ ,  $P=0.063$  uncorrected), as well as between reduced DBH<sup>+</sup> load and increased LC noradrenergic fiber load in the PD group only ( $r=0.50$ ,  $P=0.071$  uncorrected) (Table 2).



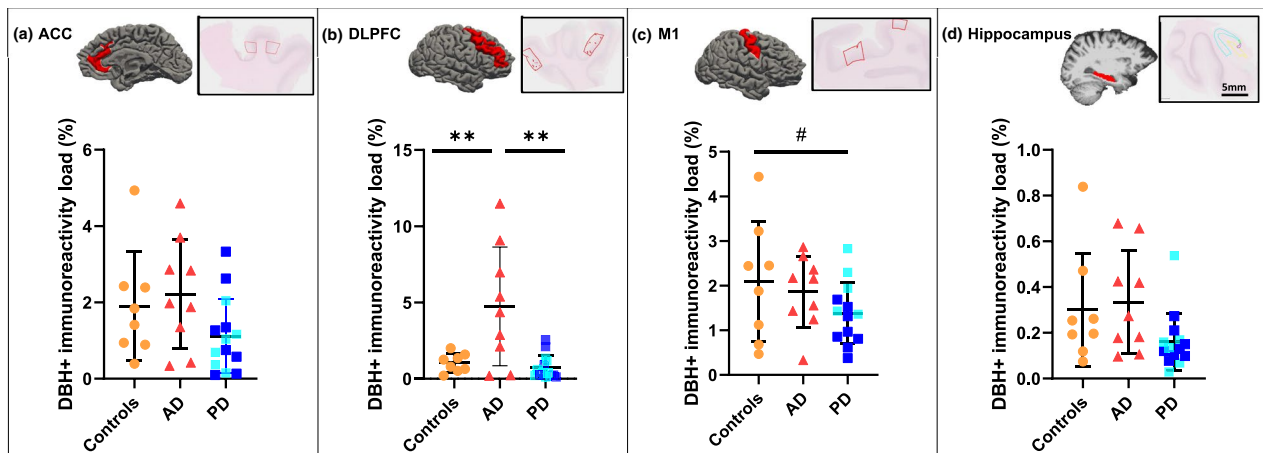


**Fig. 4** Noradrenergic innervation in the ACC, DLPFC, M1 and hippocampus. **a** PD showed a trend of reduced DBH<sup>+</sup> load in the ACC compared to AD ( $P=0.061$ , uncorrected), while no difference was found between AD and controls. **b** AD showed significantly increased DBH<sup>+</sup> load in the DLPFC compared to both PD and control donors (respectively,  $P=0.006$  and  $P=0.007$ , both FDR-corrected), while no difference was found between PD and controls. **c** PD showed reduced DBH<sup>+</sup> load in the M1 compared to controls ( $P=0.03$ , uncorrected), while no difference was found between AD and PD or between AD and controls. **d** No group differences in the DBH<sup>+</sup> load in the hippocampus was found. Within the PD group, PD cases are labeled with darker blue, whereas PDD cases are labeled with lighter blue. Scale bar, 5 mm. # $P < 0.05$ , uncorrected; \*\* $P < 0.01$ , FDR-corrected

**Diffusion MRI-measured alterations in the LC and its tracts reflect LC neuronal loss**

Within the whole cohort, we found that an increased FA of the LC was correlated with reduced noradrenergic cell density ( $r = -0.39$ ,  $P = 0.022$ , FDR-corrected, Fig. 5a) and fiber load ( $r = -0.40$ ,  $P = 0.022$ , FDR-corrected, Fig. 5b). In the PD group, increased FA of the LC was correlated

with reduced noradrenergic fiber load ( $r = -0.64$ ,  $P = 0.045$ , FDR-corrected), but not with cell density ( $P = 0.231$ ). No correlations were found for the AD group ( $P = 0.148$  and  $P = 0.304$ , for cell density and fiber load, respectively). No correlation was found between the MD of LC with noradrenergic cell density ( $P = 0.148$ ) or fiber load ( $P = 0.304$ ).

**Table 2** Correlations of LC noradrenergic cell density and fiber load with DBH<sup>+</sup> load in the DLPFC and M1

	DLPFC DBH <sup>+</sup> load (%)	
	Pearson's <i>r</i>	<i>P</i> value
<i>AD combined with controls</i>		
LC NA cell density (counts/mm <sup>2</sup> )	-0.515	0.036*
LC NA fiber load (%)	-0.036	0.454
<i>AD</i>		
LC NA cell density (counts/mm <sup>2</sup> )	-0.406	0.212
LC NA fiber load (%)	0.028	0.479
	M1 DBH <sup>+</sup> load (%)	
	Pearson's <i>r</i>	<i>P</i> value
<i>PD combined with controls</i>		
LC NA cell density (counts/mm <sup>2</sup> )	0.468	0.063
LC NA fiber load (%)	0.376	0.114
<i>PD</i>		
LC NA cell density (counts/mm <sup>2</sup> )	-0.157	0.332
LC NA fiber load (%)	0.498	0.071

AD Alzheimer's disease, PD Parkinson's disease, LC locus coeruleus, NA noradrenergic, DBH dopamine-beta hydroxylase, DLPFC dorsolateral prefrontal cortex, M1 primary motor cortex

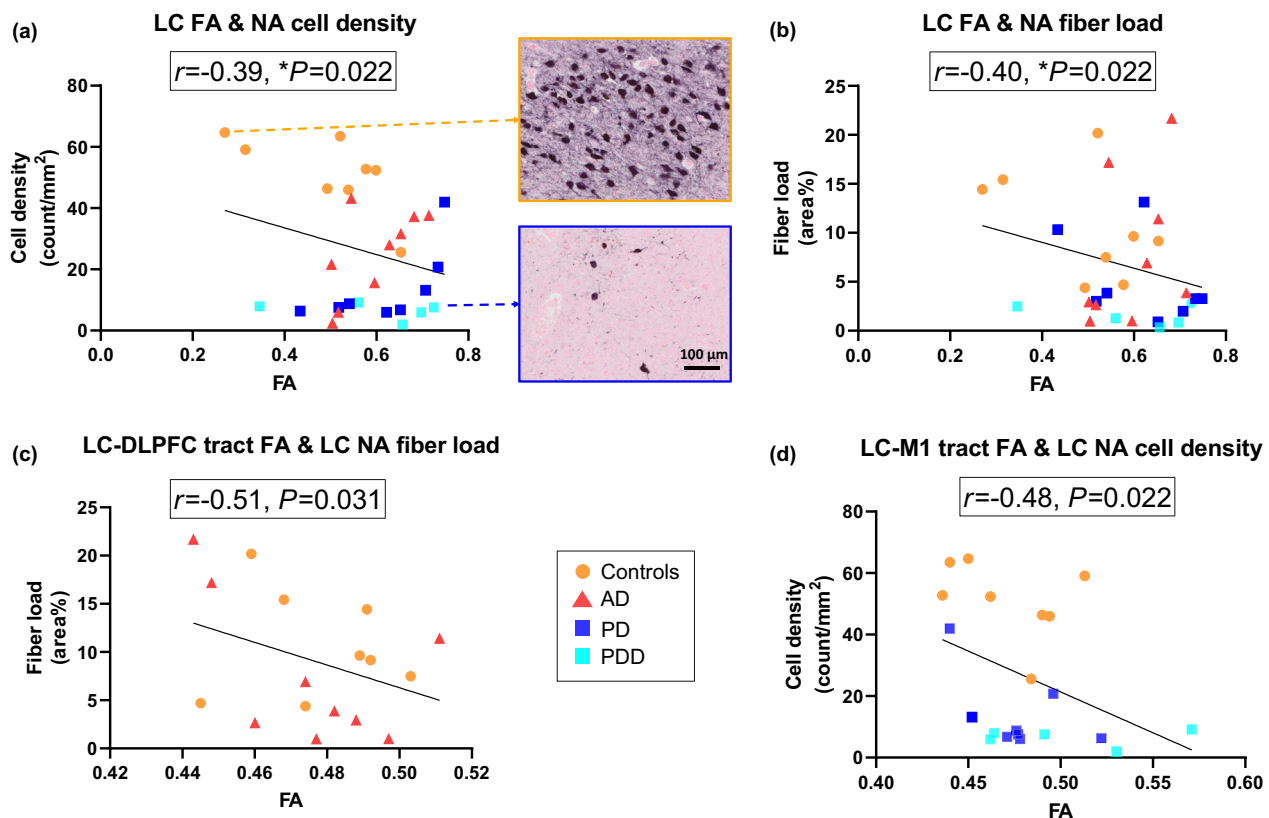


**Fig. 5** Microstructural alterations within the LC and LC-M1 tract correlate with LC-noradrenergic neuronal loss. **a** Increased FA of the LC was significantly correlated with reduced LC cell density in the whole cohort. Upper inserted image was from a control case showing low FA of the LC with high LC-noradrenergic cell density, lower image was from a PD case showing high FA of the LC with only a few LC-noradrenergic cells. Scale bar, 100  $\mu\text{m}$ . **b** Increased LC FA was significantly correlated with reduced LC noradrenergic fiber load in the whole cohort. **c** Increased FA of the LC-DLPFC tract was significantly correlated (uncorrected) with reduced LC-noradrenergic fiber load in the LC of AD and control cases. **d** Increased FA of the LC-M1 tract was significantly correlated (uncorrected) with reduced noradrenergic cell density in the LC in PD and control cases

Although we did not find any differences in MRI tract measures between groups, microscopically we observed alterations in cortical DBH-immunoreactivity within the DLPFC and M1, and LC neuronal loss, suggesting that the fiber bundles may be affected. To this end, we explored the correlations between MRI measures of the LC-DLPFC tract and the LC-M1 tract with LC noradrenergic cell density and fiber load, as well as with cortical DBH<sup>+</sup> load within the DLPFC and M1. For the LC-DLPFC tract, increased FA correlated significantly with reduced LC noradrenergic fiber load ( $r = -0.51$ ,  $P = 0.031$ ), and at the trend-level with reduced LC noradrenergic cell density ( $r = -0.48$ ,  $P = 0.054$ ) in the combined AD and control group, but not in the AD group alone. For the LC-M1 tract, increased FA significantly correlated with reduced LC noradrenergic cell density ( $r = -0.48$ ,  $P = 0.022$ , Fig. 5C) in the combined PD and control group. Within the PD group only, an increased FA showed a trend of correlation with reduced LC noradrenergic cell density ( $r = -0.52$ ,  $P = 0.063$ ). No correlations were found

between MD and LC noradrenergic cell and fiber loss, or between tract measures and cortical DBH<sup>+</sup> load (Fig. 5, Additional file 1: Table S8).

In summary, microstructural alterations of the LC-DLPFC and the LC-M1 tracts may be driven by the LC noradrenergic cell loss, rather than by noradrenergic denervation of the cortex.

## Discussion

Using a combined MRI and histopathology approach, we investigated the sensitivity of diffusion MRI measures in detecting noradrenergic degeneration within the LC and its tracts in AD and PD. On diffusion MRI, an increased FA within the LC was found in the AD group, which was correlated with a loss of LC noradrenergic cells and fibers. In addition, increased FA of the LC-to-DLPFC tract was correlated with LC-noradrenergic fiber loss in the combined AD and control group, whereas the LC-to-M1 tract was correlated with LC noradrenergic neuronal loss in the combined PD and control group. The tract

alterations were not correlated with cortical noradrenergic innervation or denervation. Altogether, our results suggest that the noradrenergic-related alterations within the LC and its tracts on diffusion MRI may be driven by the local noradrenergic neuronal loss within the LC, rather than by noradrenergic changes in the cortex.

In AD and PD, the LC undergoes severe noradrenergic neuronal loss, and aligning with previous evidence [30, 56, 67–71], we found significant loss of both noradrenergic neurons and fibers within the LC of AD and even more so in PD donors. The loss of noradrenergic neurons was not correlated with p-tau, A $\beta$  or  $\alpha$ -syn pathological hallmarks of AD or PD. While p-tau is suggested to be the main player in neuronal death in AD [72–74], the association may only be evident at early stage of the disease with less apparent neuronal loss but abundant p-tau pathology [70, 75]. In PD, the process of LB formation has been shown to associate with neurodegeneration [76–78]. In addition, both p-tau neurofibrillary tangles and  $\alpha$ -syn LBs are intracellular formations, and diminish along with cell death. Altogether, as shown in our study, both neuronal loss and pathological burden within the LC may reach a plateau at later stages of AD and PD.

We found no correlations between disease duration and noradrenergic cell density and fiber load in the LC of AD and PD donors. The results both align and contradict with previous literature [68, 79]. In the study by Zarow et al. [79], the PD disease duration was not correlated with neuronal loss in the LC but with the neuronal loss in the substantia nigra. The dopaminergic neuronal loss in the substantia nigra was shown to be associated with progression of motor severity throughout the disease [80, 81], whereas the LC is more involved at earlier stages of the disease in both cognitive and motor control. In AD, a positive correlation was found between disease duration and LC neuronal loss [68, 79], but this was not shown in our cohort, which may be due to the heterogeneity of our AD cohort, as the AD group consisted of EOAD and LOAD (Additional file 1: Fig. S6). EOAD is considered a devastating form of AD with fast deterioration of both clinical symptoms and brain pathology within a short disease duration [80, 82]. LC atrophy is greater in EOAD than in LOAD [83]. In our cohort, EOAD cases with disease duration <7 years have an average 81% loss of LC neurons, which is comparable to the LOAD with disease duration >10 years. In addition, EOAD cases with homozygous *APOE4* showed severe LC neuronal loss of 98% within only 2–6 years of disease duration (Additional file 1: Fig. S6) [84, 85]. However, this speculation was based on a descriptive observation in a very small sub-cohort of AD donors, and the interpretation requires caution [86, 87].

In our study, the FA of LC was higher in AD compared to controls, though it did not survive the correction for multiple comparisons. This may be due to the small sample size and the heterogeneity within the AD group, which consisted of EOAD and LOAD that showed differential noradrenergic degeneration when *APOE4* is taken into account. Currently, only two studies have examined LC integrity using diffusion MRI: in aging, increased FA was reported in the elderly compared to young adults [26]; in PD, higher FA was reported in patients with rapid-eye movement (REM) sleep disorder, compared to patients without this disorder, suggesting that the FA of LC is sensitive in detecting REM sleep disruptions induced by noradrenergic dysfunction at a prodromal stage of the disease. These studies indicate the capacity of FA to detect age- and disease-related alterations in the LC, as well as its connection to clinical symptoms. However, none of these studies provide a direct link towards the biological interpretation. Here, we showed that an increased FA may reflect pathological noradrenergic loss within the LC. Based on the theoretical diffusion model, the conventional interpretation of increased FA tends to be associated with increases of microstructural tissue elements, such as higher neuronal density, more intact membrane integrity and in turn less membrane permeability and greater myelination. This would be true in voxels with predominantly parallel running fibers, such as the corpus callosum. However, when the modeled FA is located at a crossing fiber region, the loss of crossing fibers would increase the FA (as a major loss in one of the crossing fiber bundles would turn the oblate tensor with a relatively low FA into a prolate tensor with a relatively high FA) in aging and neurodegeneration [25, 80, 88–91]. As the LC is located in the brainstem between the superior cerebellar peduncle, sensory nucleus trigeminal nerve, reticular formation and transverse pontine tracts, thus an environment of complex fiber architecture, loss of LC noradrenergic neurons and brainstem tracts could diminish the amount of crossing fibers [92, 93]. This would contribute to an elongated principal axis of water diffusion and thus increased FA. In contrast, MD would remain unchanged or increased with the loss of crossing fibers. We did not find group differences in the MD of LC, which may suggest that this measure is not sensitive enough in detecting noradrenergic degeneration. However, due to the small sample size and inclusion of late-stage disease donors, the results of the association of FA with neuronal loss in the LC should be interpreted with caution.

We did not find any tract difference at the group level but found correlations between tract measures and LC neuronal loss in the combined group. Previous studies

have shown increased free water and diffusivity measures of the LC–transentorhinal tract in AD, which correlate with poor memory performance and increased AD pathology in the CSF [35, 94], suggesting that diffusion MRI has the potential to capture pathological changes at an early disease stage. In our study, although tract measures did not differentiate the diseased groups from the control group, they were associated with LC neuronal loss. The lack of group difference may be due to the aforementioned small sample size and heterogeneity within the groups.

Previous studies in PD have shown reduced noradrenergic transporters in the ACC, DLPFC and hippocampus compared to controls [7, 34]. In our study, the PD donors showed a trend of lower DBH<sup>+</sup> load in these cortical regions (Fig. 4). Nonetheless, we found noradrenergic denervation in the motor cortex of PD donors compared to controls. This is consistent with previous post-mortem and in vivo imaging studies, which showed a loss of noradrenergic fibers and terminals and reduced <sup>11</sup>C-MeNER binding in the M1 region, associated with clinical motor severity and disease progression [32, 95]. In our study, the M1 noradrenergic denervation was correlated with the LC-noradrenergic cell loss. Although this correlation was at a trend-level, this may imply axonal degeneration between the LC and the M1. Supporting evidence for this was the increased FA of the LC–M1 tract and its association with the LC-noradrenergic cell loss in the combined PD and control group. This result also suggests that the tract integrity is associated with noradrenergic changes in the seed region (LC) rather than the projecting region (M1). As our cohort consisted of late-stage disease donors with a substantial loss of LC-noradrenergic neurons, the change in diffusion MRI measures in our study may reflect this late event of LC noradrenergic degeneration. The loss of noradrenergic terminals in the LC-projecting regions has been observed before the occurrence of substantial neuronal loss within the LC, implying a retrograde mechanism [56, 96–100]. Further investigations in a larger cohort with different disease stages are needed to confirm this and assess the sensitivity of diffusion MRI for early LC-noradrenergic degeneration.

In AD, cell loss within the rostral LC is expected to affect hippocampal and prefrontal noradrenergic innervation [66]. Interestingly, here we found an increased DBH-immunoreactivity in the DLPFC of AD donors and no difference in the hippocampus. Previous post-mortem studies on AD and dementia with Lewy body disease found increased mRNA expression of tyrosine hydroxylase and noradrenergic synthesis in (remaining) LC neurons, accompanied by increased  $\alpha_2$ -adrenoreceptors

and noradrenaline binding sites in the dendritic areas of the LC, hippocampus and PFC [101, 102]. This suggests noradrenergic dendritic and axonal sprouting to LC dendritic regions and projecting cortical regions. This process might be one of the compensatory mechanisms of the LC-noradrenergic system in AD [103, 104]. Results from our study may support this compensatory effect, as the sprouting of noradrenergic axon terminals, particularly in the DLPFC of AD donors, was observed (Additional file 1: Fig. S8). Unlike non-monoaminergic axons with only terminal boutons, the cortical-innervating noradrenergic axons possess beaded varicosities along the axon terminals that are in close contact to cortical interneurons and astrocytes [105]. Noradrenaline, together with densely expressed noradrenergic receptors in cortical interneurons, modulate the excitatory and inhibitory response and mediate prefrontal functioning, such as working memory and attention processing [106–110]. The axonal sprouting and increased noradrenergic immunoreactivity in the PFC of AD donors may then be the mending mechanisms for prefrontal functioning [111]. In fact, an increased CSF level of noradrenergic metabolite 3-methoxy-4-hydroxyphenylglycol (MHPG) has been found in AD patients at advanced stages of the disease [6, 112, 113], suggesting higher noradrenergic demands and turnover to support prefrontal functioning. This is an aberrant process rather than a beneficial process, as elevated MHPG levels have been associated with cognitive dysfunction as well as the spread and formation of p-tau and A $\beta$  [114]. Moreover, accumulation of p-tau and A $\beta$ , together with elevated MHPG levels, is associated with lower cortical thickness in LC-projecting regions [115]. These aberrant processes may suggest overactivation of the LC-noradrenergic circuitry for increased noradrenaline levels and a high demand on the system in neurodegenerative diseases. Nevertheless, further investigations are needed to confirm these speculations, which may aid in the development of therapeutic targets within the noradrenergic system [103].

Some limitations of this study should be addressed. First, although a sample size of 31 cases is considered large for in situ MRI-pathology studies, our results require replication in a larger cohort with donors from different stages of disease, to further validate diffusion MRI as a sensitive tool to detect noradrenergic degeneration in AD and PD. Second, although the AD and PD groups in our cohort were age- and sex-matched with controls, the inclusion of late disease stage cohort was not suitable for assessing early degeneration of the LC-noradrenergic system. In future studies, prodromal AD and preclinical PD cases are suggested to be included. The current study also shows the limitation of using LC

diffusion metrics as an (early) biomarker for AD, as no group differences or associations with pathological hallmarks were found. We assessed noradrenergic degeneration in cortical regions that are highly affected in AD and PD, but the noradrenergic axons innervate throughout the neocortex, with dense innervation to the thalamus and dentate gyrus that supports storage of synaptic information and memory formation, which can be of interest for future studies [116]. Diffusion MRI can model and assess microstructure of white matter tracts, and its diffusion markers, FA and MD, are shown to be pathologically sensitive in neurodegenerative diseases [21, 25, 117–119]. However, the signal-to-noise ratio and the partial volume effects of nearby CSF, may affect the reproducibility of FA and MD in small regions such as the LC. Although we have validated the results by fitting the FA and the MD to the data in different shells, the results of the current study require further validation using diffusion MRI with higher spatial resolution. Given the fact that the tensor model is based on one shell, which is compromised in regions where fibers cross, multi-shell models such as kurtosis imaging and neurite orientation dispersion and density imaging can be used for future studies. In addition, the LC mask registration in T1 and DWI may lead to overestimation of the LC; in turn, the extracted ROI is likely to be LC-enriched instead of LC-specific, as the average LC volume in our study is higher than the volume described in previous stereological studies [56, 64] (Additional file 1: Table S2), although our estimation is shown to be closer to the estimation in stereological studies compared to previous MRI studies [120, 121]. As an alternative, LC-sensitive MRI has a better capacity to segment the LC and differentiate the rostral and caudal LC [12], which are differentially vulnerable in AD and PD [68]. Changes of LC signal intensity on LC-sensitive MRI have been shown to be a potential biomarker for monitoring disease progression and assessing behavioral improvement on noradrenergic treatments [12, 15, 19, 20, 122–124]. Future studies are encouraged to combine LC-sensitive MRI and diffusion MRI for LC segmentation and LC tractography.

## Conclusion

In conclusion, our study was the first to show that LC-noradrenergic neuronal loss, rather than cortical noradrenergic denervation, is associated with reduced integrity of the LC and its tracts, measured by diffusion MRI, in AD and PD. Combining LC-sensitive imaging with diffusion MRI would aid in the development of sensitive tools to detect changes in the LC-noradrenergic system in neurodegenerative diseases.

## Abbreviations

LC-noradrenergic	Locus coeruleus-noradrenergic
AD	Alzheimer's disease
PD	Parkinson's disease
PDD	Parkinson's disease with dementia
FA	Fractional anisotropy
MD	Mean diffusivity
ACC	Anterior cingulate cortex
DLPFC	Dorsolateral prefrontal cortex
M1	Primary motor cortex
DBH	Dopamine-beta hydroxylase
DWI	Diffusion weighted imaging
p-tau	Phosphorylated-tau
A $\beta$	Amyloid-beta
LB	Lewy body
LN	Lewy neurite
NABCA	Normal Aging Brain Collection Amsterdam

## Supplementary Information

The online version contains supplementary material available at <https://doi.org/10.1186/s40035-024-00400-5>.

**Additional file 1: Fig. S1.** LC 3D T1 and DWI space registration and transformation in an example control case. **Fig. S2.** LC delineation and pathology quantification. **Fig. S3.** DBH staining and Qupath quantification in the cortex. **Table S1.** Detail donor information. **Table S2.** LC volume in T1 and DWI space of controls, AD and PD donors. **Table S3.** FA and MD of LC in  $b=2000$  s/mm<sup>2</sup> and  $b=1000$  s/mm<sup>2</sup> shells, and group comparison results. **Table S4.** FA and MD (b0-b2000 shell) of LC tracts to ACC, DLPFC, M1 and hippocampus in controls, AD and PD, and the group comparison. **Fig. S4.** Pathological burden within the LC in AD, PD and controls. **Fig. S5.** An AD case with  $\alpha$ -syn immunoreactivity in the LC. **Table S5.** Correlations between LC noradrenergic cell density and fiber load and pathological hallmarks. **Table S6.** Correlations between disease duration and LC noradrenergic cell density and fiber load in AD and PD. **Table S7.** Correlations between age and DBH+ whole cohort. **Fig. S6.** Correlation between disease duration and LC neuronal loss. **Fig. S7.** DBH staining pattern and noradrenergic fibers identified in ACC, DLPFC, M1 and hippocampus of controls, AD and PD. **Fig. S8.** Axonal sprouting in the DLPFC of two AD cases. **Fig. S9.** DBH staining validation with Novus (Cambridge, UK). **Table S8.** Correlations between FA and MD of the LC-DLPFC and LC-M1 tracts with LC noradrenergic cell density and fiber load. Supplementary materials for the script of LC meta mask registration using Advanced Normalization Tools (ANTs, version 2.1).

## Acknowledgements

We would like to thank all brain donors and their caregivers for donating their brains to scientific research, as well as the Netherlands Brain Bank ([www.brainbank.nl](http://www.brainbank.nl)) and the Normal Aging Brain Collection Amsterdam ([www.nabca.eu](http://www.nabca.eu); NABCA) MRI and autopsy teams for assisting data collection. Special thanks to Chris Vriend for the MRI preprocessing scripts, and Angela Ingrassia, Yvon Galis-de Graaf and Allert Jonker for helping in the lab with tissue sectioning and immunohistochemical staining.

## Author contributions

CPL contributed to experimental concept and design, data collection, MRI/pathological/statistical analysis, interpretation of the results, and drafting of the manuscript; IF, JGJB, MMAB, and AJW contributed to data collection, immunohistochemistry and pathological analysis; MJD contributed to the LC segmentation and script development on MRI; YDW contributed to experimental concept and interpretation of the results. PJWP contributed to diffusion MRI analysis optimization. WDJB and LEJ contributed to the experimental concept and design, interpretation of the results, and obtained the funding. All authors read and approved the final manuscript.

## Funding

This study was funded by The Michael J. Fox Foundation (17253). The authors have no relevant financial or non-financial interests to disclose.



**Availability of data and materials**

The datasets generated during and/or analyzed during the current study are available from the corresponding author on reasonable request. Supporting materials include supplementary methods, tables and figures.

**Declarations****Ethics approval and consent to participate**

All donors had signed an informed consent for brain donation and the use of materials and clinical information for research purposes. The procedures for brain tissue collection of NBB and NABCA have been approved by the Medical Ethical Committee of Amsterdam UMC, Vrije Universiteit Amsterdam.

**Consent for publication**

Not applicable.

**Competing interests**

The authors declare that they have no competing interests.

**Author details**

<sup>1</sup>Amsterdam UMC, Department of Anatomy and Neurosciences, Location Vrije Universiteit Amsterdam, De Boelelaan 1117, 1081 HV Amsterdam, The Netherlands. <sup>2</sup>Amsterdam Neuroscience, Brain imaging, Amsterdam, The Netherlands. <sup>3</sup>Center for Lifespan Psychology, Max Planck Institute for Human Development, 14195 Berlin, Germany. <sup>4</sup>Leonard Davis School of Gerontology, University of Southern California, Los Angeles, CA 90089, USA. <sup>5</sup>Amsterdam UMC, Department of Pathology, Location Vrije Universiteit Amsterdam, De Boelelaan 1117, Amsterdam, The Netherlands. <sup>6</sup>Amsterdam Neuroscience, Neurodegeneration, Amsterdam, The Netherlands. <sup>7</sup>Amsterdam Neuroscience, Compulsivity, Impulsivity and Attention Program, Amsterdam, The Netherlands. <sup>8</sup>Amsterdam UMC, Department of Radiology and Nuclear Medicine, Location Vrije Universiteit Amsterdam, De Boelelaan 1117, Amsterdam, The Netherlands.

Received: 15 September 2023 Accepted: 25 January 2024

Published online: 09 February 2024

**References**

- Morrison JH, Molliver ME, Grzanna R. Noradrenergic innervation of cerebral cortex: widespread effects of local cortical lesions. *Science*. 1979;205(4403):313–6.
- Borodovitsyna O, Flamini M, Chandler D. Noradrenergic modulation of cognition in health and disease. *Neural Plast*. 2017;2017:6031478.
- Dahl MJ, Mather M, Werkle-Bergner M. Noradrenergic modulation of rhythmic neural activity shapes selective attention. *Trends Cogn Sci*. 2022;26(1):38–52.
- Holland N, Robbins TW, Rowe JB. The role of noradrenaline in cognition and cognitive disorders. *Brain*. 2021;144(8):2243–56.
- Marien MR, Colpaert FC, Rosenquist AC. Noradrenergic mechanisms in neurodegenerative diseases: a theory. *Brain Res Brain Res Rev*. 2004;45(1):38–78.
- Chalermphanupap T, Kinkead B, Hu WT, Kummer MP, Hammerschmidt T, Heneka MT, et al. Targeting norepinephrine in mild cognitive impairment and Alzheimer's disease. *Alzheimers Res Ther*. 2013;5(2):21.
- Espay AJ, LeWitt PA, Kaufmann H. Norepinephrine deficiency in Parkinson's disease: the case for noradrenergic enhancement. *Mov Disord*. 2014;29(14):1710–9.
- Rommelfanger KS, Weinschenker D. Norepinephrine: the red-headed stepchild of Parkinson's disease. *Biochem Pharmacol*. 2007;74(2):177–90.
- Peterson AC, Li CR. Noradrenergic dysfunction in Alzheimer's and Parkinson's diseases—an overview of imaging studies. *Front Aging Neurosci*. 2018;10:127.
- Betts MJ, Kirilina E, Otaduy MCG, Ivanov D, Acosta-Cabronero J, Callaghan MF, et al. Locus coeruleus imaging as a biomarker for noradrenergic dysfunction in neurodegenerative diseases. *Brain*. 2019;142(9):2558–71.
- Dahl MJ, Mather M, Duzel S, Bodammer NC, Lindenberger U, Kuhn S, Werkle-Bergner M. Rostral locus coeruleus integrity is associated with better memory performance in older adults. *Nat Hum Behav*. 2019;3(11):1203–14.
- Galgani A, Lombardo F, Della Latta D, Martini N, Bonuccelli U, Fornai F, Giorgi FS. Locus coeruleus magnetic resonance imaging in neurological diseases. *Curr Neurol Neurosci Rep*. 2020;21(1):2.
- Sasaki M, Shibata E, Tohyama K, Takahashi J, Otsuka K, Tsuchiya K, et al. Neuromelanin magnetic resonance imaging of locus coeruleus and substantia nigra in Parkinson's disease. *NeuroReport*. 2006;17(11):1215–8.
- Ohtsuka C, Sasaki M, Konno K, Koide M, Kato K, Takahashi J, et al. Changes in substantia nigra and locus coeruleus in patients with early-stage Parkinson's disease using neuromelanin-sensitive MR imaging. *Neurosci Lett*. 2013;541:93–8.
- Beardmore R, Hou R, Darekar A, Holmes C, Boche D. The locus coeruleus in aging and Alzheimer's Disease: a postmortem and brain imaging review. *J Alzheimers Dis*. 2021;83(1):5–22.
- Watanabe T, Tan Z, Wang X, Martinez-Hernandez A, Frahm J. Magnetic resonance imaging of noradrenergic neurons. *Brain Struct Funct*. 2019;224(4):1609–25.
- Liu KY, Acosta-Cabronero J, Cardenas-Blanco A, Loane C, Berry AJ, Betts MJ, et al. In vivo visualization of age-related differences in the locus coeruleus. *Neurobiol Aging*. 2019;74:101–11.
- Tona KD, Keuken MC, de Rover M, Lakke E, Forstmann BU, Nieuwenhuis S, van Osch MJ. In vivo visualization of the locus coeruleus in humans: quantifying the test-retest reliability. *Brain Struct Funct*. 2017;222(9):4203–17.
- Hezemans FH, Wolpe N, O'Callaghan C, Ye R, Rua C, Jones PS, et al. Noradrenergic deficits contribute to apathy in Parkinson's disease through the precision of expected outcomes. *PLoS Comput Biol*. 2022;18(5):e1010079.
- O'Callaghan C, Hezemans FH, Ye R, Rua C, Jones PS, Murley AG, et al. Locus coeruleus integrity and the effect of atomoxetine on response inhibition in Parkinson's disease. *Brain*. 2021;144(8):2513–26.
- Lin CP, Frigerio I, Boon BDC, Zhou Z, Rozemuller AJM, Bouwman FH, et al. Structural (dys)connectivity associates with cholinergic cell density in Alzheimer's disease. *Brain*. 2022;145(8):2869–81.
- Kamagata K, Andica C, Hatano T, Ogawa T, Takeshige-Amano H, Ogaki K, et al. Advanced diffusion magnetic resonance imaging in patients with Alzheimer's and Parkinson's diseases. *Neural Regen Res*. 2020;15(9):1590–600.
- Atkinson-Clement C, Pinto S, Eusebio A, Coulon O. Diffusion tensor imaging in Parkinson's disease: review and meta-analysis. *Neuroimage Clin*. 2017;16:98–110.
- Naggara O, Oppenheim C, Rieu D, Raoux N, Rodrigo S, Dalla Barba G, Meder JF. Diffusion tensor imaging in early Alzheimer's disease. *Psychiatry Res*. 2006;146(3):243–9.
- Lin CP, Knoop LEJ, Frigerio I, Bol J, Rozemuller AJM, Berendse HW, et al. Nigral pathology contributes to microstructural integrity of striatal and frontal tracts in Parkinson's disease. *Mov Disord*. 2023.
- Langley J, Hussain S, Flores JJ, Bennett IJ, Hu X. Characterization of age-related microstructural changes in locus coeruleus and substantia nigra pars compacta. *Neurobiol Aging*. 2020;87:89–97.
- Ye Z, Rae CL, Nombela C, Ham T, Rittman T, Jones PS, et al. Predicting beneficial effects of atomoxetine and citalopram on response inhibition in Parkinson's disease with clinical and neuroimaging measures. *Hum Brain Mapp*. 2016;37(3):1026–37.
- Rae CL, Nombela C, Rodriguez PV, Ye Z, Hughes LE, Jones PS, et al. Atomoxetine restores the response inhibition network in Parkinson's disease. *Brain*. 2016;139(Pt 8):2235–48.
- Weinschenker D. Long road to ruin: noradrenergic dysfunction in neurodegenerative disease. *Trends Neurosci*. 2018;41(4):211–23.
- Benarroch EE. Locus coeruleus. *Cell Tissue Res*. 2018;373(1):221–32.
- Vermeiren Y, Van Dam D, Aerts T, Engelborghs S, Deyn De. Monoaminergic neurotransmitter alterations in postmortem brain regions of depressed and aggressive patients with Alzheimer's disease. *Neurobiol Aging*. 2014;35(12):2691–700.

32. Gaspar P, Duyckaerts C, Alvarez C, Javoy-Agid F, Berger B. Alterations of dopaminergic and noradrenergic innervations in motor cortex in Parkinson's disease. *Ann Neurol*. 1991;30(3):365–74.
33. Delaville C, Deurwaerdere PD, Benazzouz A. Noradrenaline and Parkinson's disease. *Front Syst Neurosci*. 2011;5:31.
34. Emre M. What causes mental dysfunction in Parkinson's disease? *Mov Disord*. 2003;18(Suppl 6):S63–71.
35. Sun W, Tang Y, Qiao Y, Ge X, Mather M, Ringman JM, et al. A probabilistic atlas of locus coeruleus pathways to transentorhinal cortex for connectome imaging in Alzheimer's disease. *Neuroimage*. 2020;223:117301.
36. Tang Y, Cao M, Li Y, Lin Y, Wu X, Chen M. Alzheimer's Disease Neuroimaging I. Altered structural covariance of locus coeruleus in individuals with significant memory concern and patients with mild cognitive impairment. *Cereb Cortex*. 2023;33(13):8523–33.
37. Jonkman LE, Graaf YG, Bulk M, Kaaij E, Pouwels PJW, Barkhof F, et al. Normal Aging Brain Collection Amsterdam (NABCA): a comprehensive collection of postmortem high-field imaging, neuropathological and morphometric datasets of non-neurological controls. *Neuroimage Clin*. 2019;22: 101698.
38. Postuma RB, Berg D, Stern M, Poewe W, Olanow CW, Oertel W, et al. MDS clinical diagnostic criteria for Parkinson's disease. *Mov Disord*. 2015;30(12):1591–601.
39. McKeith IG, Boeve BF, Dickson DW, Halliday G, Taylor JP, Weintraub D, et al. Diagnosis and management of dementia with Lewy bodies: Fourth consensus report of the DLB Consortium. *Neurology*. 2017;89(1):88–100.
40. Emre M, Aarsland D, Brown R, Burn DJ, Duyckaerts C, Mizuno Y, et al. Clinical diagnostic criteria for dementia associated with Parkinson's disease. *Mov Disord*. 2007;22(12):1689–707.
41. Klioueva NM, Rademaker MC, Dexter DT, Al-Sarraj S, Seilhean D, Streichenberger N, et al. BrainNet Europe's code of conduct for brain banking. *J Neural Transm*. 2015;122(7):937–40.
42. Steenwijk MD, Pouwels PJ, Daams M, van Dalen JW, Caan MW, Richard E, et al. Accurate white matter lesion segmentation by k nearest neighbor classification with tissue type priors (kNN-TTPs). *Neuroimage Clin*. 2013;3:462–9.
43. Smith SM, Jenkinson M, Woolrich MW, Beckmann CF, Behrens TE, Johansen-Berg H, et al. Advances in functional and structural MR image analysis and implementation as FSL. *Neuroimage*. 2004;23(Suppl 1):S208–19.
44. Dahl MJ, Mather M, Werkle-Bergner M, Kennedy BL, Guzman S, Hurth K, et al. Locus coeruleus integrity is related to tau burden and memory loss in autosomal-dominant Alzheimer's disease. *Neurobiol Aging*. 2022;112:39–54.
45. Tustison NJ, Avants BB, Gee JC. Directly manipulated free-form deformation image registration. *IEEE Trans Image Process*. 2009;18(3):624–35.
46. Avants BB, Tustison NJ, Song G, Cook PA, Klein A, Gee JC. A reproducible evaluation of ANTs similarity metric performance in brain image registration. *Neuroimage*. 2011;54(3):2033–44.
47. Dale AM, Fischl B, Sereno MI. Cortical surface-based analysis. I Segment Surface Reconstr. *Neuroimage*. 1999;9(2):179–94.
48. Greve DN, Fischl B. Accurate and robust brain image alignment using boundary-based registration. *Neuroimage*. 2009;48(1):63–72.
49. Tournier JD, Smith R, Raffelt D, Tabbara R, Dhollander T, Pietsch M, et al. MRtrix3: a fast, flexible and open software framework for medical image processing and visualisation. *Neuroimage*. 2019;202:116137.
50. Andersson JLR, Sotiropoulos SN. An integrated approach to correction for off-resonance effects and subject movement in diffusion MR imaging. *Neuroimage*. 2016;125:1063–78.
51. Basser PJ, Mattiello J, LeBihan D. MR diffusion tensor spectroscopy and imaging. *Biophys J*. 1994;66(1):259–67.
52. Vriend C, van Balkom TD, Berendse HW, van der Werf YD, van den Heuvel OA. Cognitive training in Parkinson's disease induces local, not global. Changes in white matter microstructure. *Neurotherapeutics*. 2021;18(4):2518–28.
53. Jeurissen B, Tournier JD, Dhollander T, Connelly A, Sijbers J. Multi-tissue constrained spherical deconvolution for improved analysis of multi-shell diffusion MRI data. *Neuroimage*. 2014;103:411–26.
54. Frigerio I, Laansma MA, Lin CP, Hermans EJM, Bouwman MMA, Bol J, et al. Neurofilament light chain is increased in the parahippocampal cortex and associates with pathological hallmarks in Parkinson's disease dementia. *Transl Neurodegener*. 2023;12(1):3.
55. Adler DH, Pluta J, Kadivar S, Craige C, Gee JC, Avants BB, Yushkevich PA. Histology-derived volumetric annotation of the human hippocampal subfields in postmortem MRI. *Neuroimage*. 2014;84:505–23.
56. Theofilas P, Ehrenberg AJ, Dunlop S, Di Lorenzo Alho AT, Nguy A, Leite REP, et al. Locus coeruleus volume and cell population changes during Alzheimer's disease progression: a stereological study in human postmortem brains with potential implication for early-stage biomarker discovery. *Alzheimers Dement*. 2017;13(3):236–46.
57. Loughlin SE, Foote SL, Bloom FE. Efferent projections of nucleus locus coeruleus: topographic organization of cells of origin demonstrated by three-dimensional reconstruction. *Neuroscience*. 1986;18(2):291–306.
58. Bankhead P, Loughrey MB, Fernandez JA, Dombrowski Y, McArt DG, Dunne PD, et al. QuPath: open source software for digital pathology image analysis. *Sci Rep*. 2017;7(1):16878.
59. Ohm DT, Peterson C, Lobrovich R, Cousins KAQ, Gibbons GS, McMillan CT, et al. Degeneration of the locus coeruleus is a common feature of tauopathies and distinct from TDP-43 proteinopathies in the frontotemporal lobar degeneration spectrum. *Acta Neuropathol*. 2020;140(5):675–93.
60. Bogerts B. A brainstem atlas of catecholaminergic neurons in man, using melanin as a natural marker. *J Comp Neurol*. 1981;197(1):63–80.
61. Frigerio I, Boon BDC, Lin CP, Galis-de Graaf Y, Bol J, Preziosa P, et al. Amyloid-beta, p-tau and reactive microglia are pathological correlates of MRI cortical atrophy in Alzheimer's disease. *Brain Commun*. 2021;3(4):281.
62. Arendt T, Morawski M, Gartner U, Frohlich N, Schulze F, Wohmann N, et al. Inhomogeneous distribution of Alzheimer pathology along the isocortical relief. Are cortical convolutions an Achilles heel of evolution? *Brain Pathol*. 2017;27(5):603–11.
63. Zarkali A, McColgan P, Leyland LA, Lees AJ, Rees G, Weil RS. Fiber-specific white matter reductions in Parkinson hallucinations and visual dysfunction. *Neurology*. 2020;94(14):e1525–38.
64. Fernandes P, Regala J, Correia F, Goncalves-Ferreira AJ. The human locus coeruleus 3-D stereotactic anatomy. *Surg Radiol Anat*. 2012;34(10):879–85.
65. Kauffman S, Friedman S. Dopamine-beta-hydroxylase. *Pharmacol Rev*. 1965;17:71–100.
66. Powers RE, Struble RG, Casanova MF, O'Connor DT, Kitt CA, Price DL. Innervation of human hippocampus by noradrenergic systems: normal anatomy and structural abnormalities in aging and in Alzheimer's disease. *Neuroscience*. 1988;25(2):401–17.
67. Chan-Palay V. Alterations in the locus coeruleus in dementias of Alzheimer's and Parkinson's disease. *Prog Brain Res*. 1991;88:625–30.
68. German DC, Manaye KF, White CL 3rd, Woodward DJ, McIntire DD, Smith WK, et al. Disease-specific patterns of locus coeruleus cell loss. *Ann Neurol*. 1992;32(5):667–76.
69. Gesi M, Soldani P, Giorgi FS, Santinami A, Bonaccorsi I, Fornai F. The role of the locus coeruleus in the development of Parkinson's disease. *Neurosci Biobehav Rev*. 2000;24(6):655–68.
70. Chen Y, Chen T, Hou R. Locus coeruleus in the pathogenesis of Alzheimer's disease: a systematic review. *Alzheimers Dement*. 2022;8(1):e12257.
71. Gilvesy A, Husen E, Magloczky Z, Mihaly O, Hortobagyi T, Kanatani S, et al. Spatiotemporal characterization of cellular tau pathology in the human locus coeruleus-pericoeruleus complex by three-dimensional imaging. *Acta Neuropathol*. 2022;144(4):651–76.
72. Thal DR, Tome SO. The central role of tau in Alzheimer's disease: from neurofibrillary tangle maturation to the induction of cell death. *Brain Res Bull*. 2022;190:204–17.
73. Mandelkow EM, Mandelkow E. Tau in Alzheimer's disease. *Trends Cell Biol*. 1998;8(11):425.
74. Kobayashi K, Nakano H, Hayashi M, Shimazaki M, Fukutani Y, Sasaki K, et al. Association of phosphorylation site of tau protein with neuronal apoptosis in Alzheimer's disease. *J Neurol Sci*. 2003;208(1–2):17–24.
75. Huynh B, Fu Y, Kirik D, Shine JM, Halliday GM. Comparison of locus coeruleus pathology with nigral and forebrain pathology in Parkinson's disease. *Mov Disord*. 2021;36(9):2085–93.

76. Dickson DW. Linking selective vulnerability to cell death mechanisms in Parkinson's disease. *Am J Pathol.* 2007;170(1):16–9.
77. Cookson MR. alpha-Synuclein and neuronal cell death. *Mol Neurodegener.* 2009;4:9.
78. Mahul-Mellier AL, Bartscher J, Maharjan N, Weerens L, Croisier M, Kuttler F, et al. The process of Lewy body formation, rather than simply alpha-synuclein fibrillization, is one of the major drivers of neurodegeneration. *Proc Natl Acad Sci U S A.* 2020;117(9):4971–82.
79. Zarow C, Lyness SA, Mortimer JA, Chui HC. Neuronal loss is greater in the locus coeruleus than nucleus basalis and substantia nigra in Alzheimer and Parkinson diseases. *Arch Neurol.* 2003;60(3):337–41.
80. Kordower JH, Olanow CW, Dodiya HB, Chu Y, Beach TG, Adler CH, et al. Disease duration and the integrity of the nigrostriatal system in Parkinson's disease. *Brain.* 2013;136(Pt 8):2419–31.
81. Greffard S, Verry M, Bonnet A-M, Beinis J-Y, Gallinari C, Meaume S, et al. Motor Score of the unified Parkinson disease rating scale as a good predictor of Lewy body-associated neuronal loss in the substantia nigra. *Arch Neurol.* 2006;63(4):584–8.
82. Koedam EL, Lauffer V, van der Vlies AE, van der Flier WM, Scheltens P, Pijnenburg YA. Early-versus late-onset Alzheimer's disease: more than age alone. *J Alzheimers Dis.* 2010;19(4):1401–8.
83. Bolton CJ, Tam JW. Differential involvement of the locus coeruleus in early- and late-onset Alzheimer's disease: a potential mechanism of clinical differences? *J Geriatr Psychiatry Neurol.* 2022;35(5):733–9.
84. Mendez MF. Early-onset Alzheimer disease and its variants. *Continuum.* 2019;25(1):34–51.
85. Sirkis DW, Bonham LW, Johnson TP, La Joie R, Yokoyama JS. Dissecting the clinical heterogeneity of early-onset Alzheimer's disease. *Mol Psychiatry.* 2022;27(6):2674–88.
86. 2021 Alzheimer's disease facts and figures. *Alzheimers Dement.* 2021;17(3):327–406.
87. Bondareff W, Mountjoy CQ, Roth M, Rossor MN, Iversen LL, Reynolds GP. Age and histopathologic heterogeneity in Alzheimer's disease. *Evid Subtypes Arch Gen Psychiatry.* 1987;44(5):412–7.
88. Teipel SJ, Grothe MJ, Filippi M, Fellgiebel A, Dyrba M, Frisoni GB, et al. Fractional anisotropy changes in Alzheimer's disease depend on the underlying fiber tract architecture: a multiparametric DTI study using joint independent component analysis. *J Alzheimers Dis.* 2014;41(1):69–83.
89. Stahon KE, Bastian C, Griffith S, Kidd GJ, Brunet S, Baltan S. Age-related changes in axonal and mitochondrial ultrastructure and function in white matter. *J Neurosci.* 2016;36(39):9990–10001.
90. Figley CR, Uddin MN, Wong K, Kornelsen J, Puig J, Figley TD. Potential pitfalls of using fractional anisotropy, axial diffusivity, and radial diffusivity as biomarkers of cerebral white matter microstructure. *Front Neurosci.* 2021;15:799576.
91. Budde MD, Janes L, Gold E, Turtzo LC, Frank JA. The contribution of gliosis to diffusion tensor anisotropy and tractography following traumatic brain injury: validation in the rat using Fourier analysis of stained tissue sections. *Brain.* 2011;134(Pt 8):2248–60.
92. Muller SJ, Khadhraoui E, Hansen N, Jamous A, Langer P, Wiltfang J, et al. Brainstem atrophy in dementia with Lewy bodies compared with progressive supranuclear palsy and Parkinson's disease on MRI. *BMC Neurol.* 2023;23(1):114.
93. Hilal S, Amin SM, Venketasubramanian N, Niessen WJ, Vrooman H, Wong TY, et al. Subcortical atrophy in cognitive impairment and dementia. *J Alzheimers Dis.* 2015;48(3):813–23.
94. Chu WT, Wang WE, Zaborszky L, Golde TE, DeKosky S, Duara R, et al. Association of cognitive impairment with free water in the nucleus basalis of Meynert and locus coeruleus to transentorhinal cortex tract. *Neurology.* 2022;98(7):e700–10.
95. Sommerauer M, Hansen AK, Parbo P, Fedorova TD, Knudsen K, Frederiksen Y, et al. Decreased noradrenaline transporter density in the motor cortex of Parkinson's disease patients. *Mov Disord.* 2018;33(6):1006–10.
96. Sotiriou E, Vassiliadis DK, Vila M, Stefanis L. Selective noradrenergic vulnerability in alpha-synuclein transgenic mice. *Neurobiol Aging.* 2010;31(12):2103–14.
97. Palmer AM, Wilcock GK, Esiri MM, Francis PT, Bowen DM. Monoaminergic innervation of the frontal and temporal lobes in Alzheimer's disease. *Brain Res.* 1987;401(2):231–8.
98. Trillo L, Das D, Hsieh W, Medina B, Moghadam S, Lin B, et al. Ascending monoaminergic systems alterations in Alzheimer's disease translating basic science into clinical care. *Neurosci Biobehav Rev.* 2013;37(8):1363–79.
99. Doppler CEJ, Kinnerup MB, Brune C, Farrher E, Betts M, Fedorova TD, et al. Regional locus coeruleus degeneration is uncoupled from noradrenergic terminal loss in Parkinson's disease. *Brain.* 2021;144(9):2732–44.
100. Helmich RC, Lehericy S. Dying-back of ascending noradrenergic projections in Parkinson's disease. *Brain.* 2021;144(9):2562–4.
101. Szot P, White SS, Greenup JL, Leverenz JB, Peskind ER, Raskind MA. Changes in adrenoceptors in the prefrontal cortex of subjects with dementia: evidence of compensatory changes. *Neuroscience.* 2007;146(1):471–80.
102. Szot P, White SS, Greenup JL, Leverenz JB, Peskind ER, Raskind MA. Compensatory changes in the noradrenergic nervous system in the locus coeruleus and hippocampus of postmortem subjects with Alzheimer's disease and dementia with Lewy bodies. *J Neurosci.* 2006;26(2):467–78.
103. Matchett BJ, Grinberg LT, Theofilas P, Murray ME. The mechanistic link between selective vulnerability of the locus coeruleus and neurodegeneration in Alzheimer's disease. *Acta Neuropathol.* 2021;141(5):631–50.
104. Gannon M, Che P, Chen Y, Jiao K, Roberson ED, Wang Q. Noradrenergic dysfunction in Alzheimer's disease. *Front Neurosci.* 2015;9:220.
105. Wahis J, Holt MG. Astrocytes, noradrenaline, alpha1-adrenoceptors, and neuromodulation: evidence and unanswered questions. *Front Cell Neurosci.* 2021;15:645691.
106. Briand LA, Gritton H, Howe WM, Young DA, Sarter M. Modulators in concert for cognition: modulator interactions in the prefrontal cortex. *Prog Neurobiol.* 2007;83(2):69–91.
107. Paspalas CD, Papadopoulos GC. Noradrenergic innervation of peptidergic interneurons in the rat visual cortex. *Cereb Cortex.* 1999;9(8):844–53.
108. Labarrera C, Deitcher Y, Dudai A, Weiner B, Kaduri Amichai A, Zylbermann N, London M. Adrenergic modulation regulates the dendritic excitability of layer 5 pyramidal neurons in vivo. *Cell Rep.* 2018;23(4):1034–44.
109. Yan Z, Rein B. Mechanisms of synaptic transmission dysregulation in the prefrontal cortex: pathophysiological implications. *Mol Psychiatry.* 2022;27(1):445–65.
110. Arnsten AF, Li BM. Neurobiology of executive functions: catecholamine influences on prefrontal cortical functions. *Biol Psychiatry.* 2005;57(11):1377–84.
111. Xiao Z, Deng PY, Rojanathammanee L, Yang C, Grisanti L, Permpoonputtana K, et al. Noradrenergic depression of neuronal excitability in the entorhinal cortex via activation of TREK-2 K<sup>+</sup> channels. *J Biol Chem.* 2009;284(16):10980–91.
112. Hoogendijk WJ, Feenstra MG, Botterblom MH, Gilhuis J, Sommer IE, Kamphorst W, et al. Increased activity of surviving locus coeruleus neurons in Alzheimer's disease. *Ann Neurol.* 1999;45(1):82–91.
113. Raskind MA, Peskind ER, Halter JB, Jimerson DC. Norepinephrine and MHPG levels in CSF and plasma in Alzheimer's disease. *Arch Gen Psychiatry.* 1984;41(4):343–6.
114. Ross JA, McGonigle P, Van Bockstaele EJ. Locus Coeruleus, norepinephrine and Abeta peptides in Alzheimer's disease. *Neurobiol Stress.* 2015;2:73–84.
115. van Hooren RWE, Verhey FRJ, Ramakers I, Jansen WJ, Jacobs HIL. Elevated norepinephrine metabolism is linked to cortical thickness in the context of Alzheimer's disease pathology. *Neurobiol Aging.* 2021;102:17–22.
116. Hagen H, Hansen N, Manahan-Vaughan D. beta-adrenergic control of hippocampal function: subserving the choreography of synaptic information storage and memory. *Cereb Cortex.* 2016;26(4):1349–64.
117. Li KR, Wu AG, Tang Y, He XP, Yu CL, Wu JM, et al. The Key Role of magnetic resonance imaging in the detection of neurodegenerative diseases-associated biomarkers: a review. *Mol Neurobiol.* 2022;59(10):5935–54.
118. Chen Y, Wang Y, Song Z, Fan Y, Gao T, Tang X. Abnormal white matter changes in Alzheimer's disease based on diffusion tensor imaging: A systematic review. *Ageing Res Rev.* 2023;87:101911.
119. Kamagata K, Andica C, Kato A, Saito Y, Uchida W, Hatano T, et al. Diffusion magnetic resonance imaging-based biomarkers for neurodegenerative diseases. *Int J Mol Sci.* 2021;22:10.

120. Chen X, Huddleston DE, Langley J, Ahn S, Barnum CJ, Factor SA, et al. Simultaneous imaging of locus coeruleus and substantia nigra with a quantitative neuromelanin MRI approach. *Magn Reson Imaging*. 2014;32(10):1301–6.
121. Ye R, Rua C, O'Callaghan C, Jones PS, Hezemans FH, Kaalund SS, et al. An in vivo probabilistic atlas of the human locus coeruleus at ultra-high field. *Neuroimage*. 2021;225:117487.
122. Cho SJ, Bae YJ, Kim JM, Kim D, Baik SH, Sunwoo L, et al. Diagnostic performance of neuromelanin-sensitive magnetic resonance imaging for patients with Parkinson's disease and factor analysis for its heterogeneity: a systematic review and meta-analysis. *Eur Radiol*. 2021;31(3):1268–80.
123. He N, Chen Y, LeWitt PA, Yan F, Haacke EM. Application of neuromelanin MR imaging in Parkinson disease. *J Magn Reson Imaging*. 2023;57(2):337–52.
124. Galgani A, Lombardo F, Martini N, Vergallo A, Bastiani L, Hampel H, et al. Magnetic resonance imaging Locus Coeruleus abnormality in amnesic mild cognitive impairment is associated with future progression to dementia. *Eur J Neurol*. 2023;30(1):32–46.